ARL2BP, a protein linked to retinitis pigmentosa, is needed for normal photoreceptor cilia doublets and outer segment structure

Abigail R. Moye[a,b], Ratnesh Singh[b], Victoria A. Kimler[c], Tanya L. Dilan[a,b], Daniella Munezero[a,b], Thamaraiselvi Saravanan[a], Andrew F. X. Goldberg[c], and Visvanathan Ramamurthy[a,b,d,*]

[a]Department of Ophthalmology, [b]Department of Biochemistry, and [d]Rockefeller Neurosciences Institute, West Virginia University, Morgantown, WV 26506; [c]Eye Research Institute, Oakland University, Rochester, MI 48309

ABSTRACT **The outer segment (OS) of photoreceptor cells is an elaboration of a primary cilium with organized stacks of membranous disks that contain the proteins needed for phototransduction and vision. Though ciliary formation and function has been well characterized, little is known about the role of cilia in the development of photoreceptor OS. Nevertheless, progress has been made by studying mutations in ciliary proteins, which often result in malformed OSs and lead to blinding diseases. To investigate how ciliary proteins contribute to OS formation, we generated a knockout (KO) mouse model for ARL2BP, a ciliary protein linked to retinitis pigmentosa. The KO mice display an early and progressive reduction in visual response. Before photoreceptor degeneration, we observed disorganization of the photoreceptor OS, with vertically aligned disks and shortened axonemes. Interestingly, ciliary doublet microtubule (MT) structure was also impaired, displaying open B-tubule doublets, paired with loss of singlet MTs. On the basis of results from this study, we conclude that ARL2BP is necessary for photoreceptor ciliary doublet formation and axoneme elongation, which is required for OS morphogenesis and vision.**

Monitoring Editor
Erika Holzbaur
University of Pennsylvania

Received: Jan 18, 2018
Revised: Apr 23, 2018
Accepted: Apr 27, 2018

INTRODUCTION

Photoreceptors are ciliated neurons that absorb photons and convert light into electrical signals. These neurons are compartmentalized with outer and inner segments (OS and IS) bridged by a narrow connecting cilium (CC, corresponds to the ciliary transition zone) with an extended axoneme (Pearring *et al.*, 2013; Goldberg *et al.*, 2016; May-Simera *et al.*, 2017). The OS contains stacked membranous disks that anchor proteins that participate in phototransduction (Molday and Moritz, 2015). Remarkably, photoreceptors shed 10% of their disks every day (Young, 1967; Goldberg *et al.*, 2016). To maintain the OSs, photoreceptors need to ensure continuous transport of proteins and membranes from their site of synthesis in the IS through the CC to the OS (Young, 1967). In addition to facilitating protein movement, the photoreceptor axoneme is thought to play a structural role in the formation and continual replacement of OS disks (Liu *et al.*, 2004).

Though the photoreceptor cilium is highly modified in function, the basic structure is consistent with immotile primary cilia seen in other tissues, containing 9 + 0 MT morphology that undergoes a switch from doublet microtubules (DMTs) to singlet MTs approximately one-third of the way up the axoneme (Brown *et al.*, 1963; Steinberg and Wood, 1975; Knabe and Kuhn, 1997; Insinna *et al.*, 2008; Wensel *et al.*, 2016). The axonemal DMTs consist of an A-tubule containing 13 tubulin protofilaments joined to a B-tubule containing 10 tubulin protofilaments, with an 11th nontubulin complex linking the inner junction of A and B tubules (see Figure 7A later in this article) (Linck and Stephens, 2007; Nicastro *et al.*, 2011; Pigino *et al.*, 2012; Linck *et al.*, 2014; Ichikawa *et al.*, 2017). Defects in the

This article was published online ahead of print in MBoC in Press (http://www.molbiolcell.org/cgi/doi/10.1091/mbc.E18-01-0040) on May 2, 2018.

*Address correspondence to: Visvanathan Ramamurthy (ramamurthyv@wvumedicine.org)

Abbreviations used: AcTu, acetylated tubulin; ARL2, ADP-ribosylation factor-like 2; ARL2BP, ADP-ribosylation factor-like protein 2 binding partner; BB, basal body; CC, connecting cilium; CNGA-1, cyclic nucleotide-gated channel α1; DMT, doublet microtubules; ERG, electroretinogram; GαT1, transducin; IS, photoreceptor inner segment; KO, knockout; mAb, monoclonal antibody; MAK, male germ cell–associated kinase; MIP, MT-interacting protein; MT, microtubule; OS, photoreceptor outer segment; PAM, protospacer adjacent motif; PBS, phosphate-buffered saline; PDE6β, phosphodiesterase-6β; PFA, paraformaldehyde; PRPH-2, peripherin-2/Rds; RHO, rhodopsin; RP, retinitis pigmentosa; RP1, retinitis pigmentosa-1; RPGR, retinitis pigmentosa GTPase regulator; STX3, syntaxin 3; TEM, transmission electron microscopy; WT, wild type.

structural integrity of photoreceptor CC/axoneme lead to retinal degenerative diseases such as retinitis pigmentosa (RP), Lebers congenital amaurosis, and multiple ciliopathies (Pierce *et al.*, 1999; Ramamurthy and Cayouette, 2009; Omori *et al.*, 2010; Boldt *et al.*, 2011; Bujakowska *et al.*, 2017). For example, mice lacking retinitis pigmentosa 1 (RP1), a protein that links the OS disks to the axoneme, displayed shortened axonemes and disordered OS disk structure (Liu *et al.*, 2003, 2004). Conversely, the absence of male germ-cell associated kinase (MAK) in murine retina resulted in extended axonemes, as well as disorganized OS disks (Omori *et al.*, 2010). Despite the importance of the ciliary axoneme in photoreceptor structure and function, relatively little is known of the mechanism and players behind ciliogenesis and disk organization in the OS.

ADP-ribosylation factor-like 2 binding protein (ARL2BP) is a protein present in the CC and basal body (BB) regions of photoreceptor cells (Davidson *et al.*, 2013); however, the role for ARL2BP in photoreceptors is unknown. In cultured cells, ARL2BP was found specifically localized to the centrosome and midbody of actively dividing cells (Zhou *et al.*, 2006). Additionally, the knockdown of ARL2BP expression in ARPE-19 cells produced a modest reduction in the length of primary cilia, suggesting a role for ARL2BP in ciliogenesis (Davidson *et al.*, 2013).

There are multiple pathogenic mutations in ARL2BP leading to blindness, one of which is a recessive splice site mutation leading to premature termination of the gene (Davidson *et al.*, 2013). To model RP and determine the role for ARL2BP, we generated a mouse knockout (KO) of ARL2BP using the CRISPR-Cas9 system. Findings from this study corroborate the phenotype evident in patients, displaying photoreceptor dysfunction with loss of ARL2BP. Our data further establish a photoreceptor-specific role for ARL2BP in axoneme length regulation, disk morphogenesis, and ciliary doublet formation.

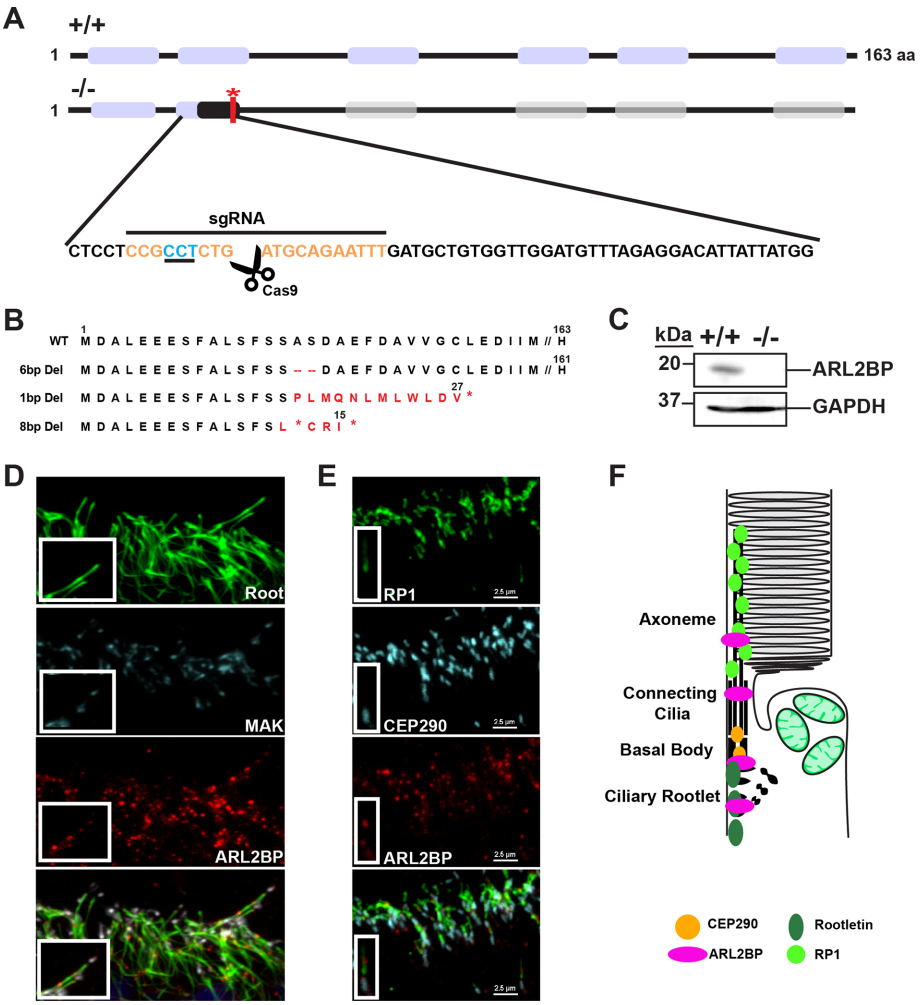

FIGURE 1: Endogenous ARL2BP expression and generation of KO model. (A) Scheme illustrating mutations generated by the Crispr-Cas9 system in ARL2BP. Exon 2 is magnified, showing the sgRNA target locus where Cas9 generates a double-stranded break. The PAM for Cas9 is indicated in blue. (B) Nonhomologous end joining (NHEJ) following the Cas9 cleavage led to multiple mutations. In two of the mutants, 1– and 8–base pair deletions (bp del) were found, causing a frameshift mutation and early stop codon (red asterisk). In the third mutant, there was an in-frame 6–base pair deletion, producing loss of two amino acids. The red asterisk marks stop in protein. (C) Immunoblot analysis of endogenous ARL2BP protein levels in P16 retinal tissues using ARL2BP and GAPDH (loading control) directed antibodies. Protein molecular weight in kilodaltons (kDa) is indicated on the left. $n = 3$; WT (+/+), KO (–/–). (D, E) Retinal cross-sections from WT (+/+) mice at P25 showing localization for ARL2BP (red) in relation to (D) rootletin (Root, green) and MAK (cyan), and (E) retinitis pigmentosa 1 (RP1, green) and centrosomal protein of 290 kDa (CEP290, cyan). Scale bar = 2.5 µm. (F) Scheme illustrating the localization of ciliary proteins and ARL2BP in photoreceptors based on the results from D and E.

RESULTS

Generation of ARL2BP KO mice

We used the CRISPR-Cas9 system to create a global KO of ARL2BP (scheme illustrated in Figure 1A). Three homozygous mouse lines—a 6–base pair, a 1–base pair, and an 8–base pair deletion in ARL2BP—were identified. The 6–base pair deletion line produced an in-frame removal of two amino acids (Δ16–17 amino acid residues, Figure 1B). Both the 1–base pair and 8–base pair deletions caused a frameshift mutation and led to a premature termination (Figure 1B). These two lines are reminiscent of one of the patient mutations, splice site variant mutation in ARL2BP, which also caused ablation of the protein (Davidson *et al.*, 2013). The ARL2BP-null mice were comparable in weight and development to wild-type (WT) littermates, with no detectable health issues.

To demonstrate the removal of ARL2BP protein in our 1– and 8–base pair deletion animal models, we generated a rabbit antibody against full-length mouse ARL2BP protein. Immunoblot analysis using this antibody and a commercially available monoclonal antibody (mAb) on retinal lysates at P30 from WT and ARL2BP KO littermates confirmed the absence of ARL2BP in KO animals (Figure 1C and Supplemental Figure 1B). For the remainder of this study, unless otherwise stated, ARL2BP KO mice will refer to mice possessing an 8–base pair deletion. Localization of ARL2BP in the retina was established using a mAb, showing punctate staining of ARL2BP in the IS, BB, and CC of photoreceptors (Figure 1, D and E). This is consistent with the localization presented in a published study using immunoelectron microscopy (scheme illustrated in Figure 1F)

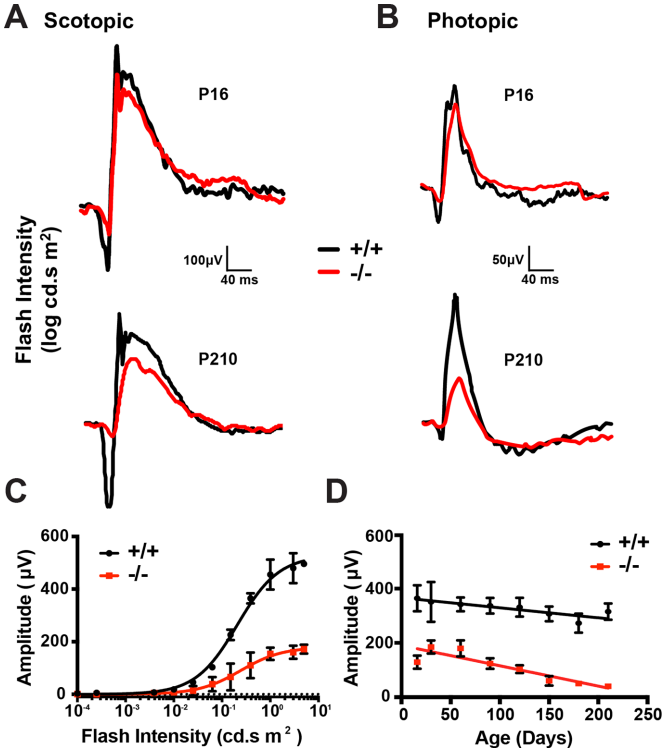

FIGURE 2: Decreased photoreceptor function in animals lacking ARL2BP. (A, B) Representative scotopic (rod, A) and photopic (cone, B) ERGs at –0.8 cd · s m^{-2} (A) and 0.69 cd · s m^{-2} (B) comparing WT (+/+) and KO (–/–) animals at P16 and P210. (C) Intensity-response relationships for scotopic "a" waves recorded at P16 between +/+ and –/–. The data were fitted with a hyperbolic function to define scotopic "a"-wave half-saturating light intensities of 0.2075 ± 0.02 cd · s m^{-2} (+/+, $n = 4$) and 0.241 ± 0.06 cd · s m^{-2} (–/–, $n = 4$) and "a"-wave maximum amplitudes of 528.4 ± 12.93 μV (+/+, $n = 4$) and 179.8 ± 10.48 μV (–/–, $n = 4$). (D) Scotopic "a"-wave amplitude measured at the light intensity of –0.8 cd · s m^{-2} across multiple ages between +/+ and –/–. Data for C and D are represented as mean ± SEM ($n = 4$, unpaired two-tailed t test; all were statistically significant, $p < 0.05$). All experiments were conducted with littermate controls.

(Davidson *et al.*, 2013). The localization of ARL2BP was further confirmed by exogenous expression of subretinally injected epitope-tagged ARL2BP (Supplemental Figure 1C).

ARL2BP is essential for efficient photoresponse

Photoreceptor function was assessed in WT and KO littermates using electroretinogram (ERG) recordings, an established technique that measures the hyperpolarization generated by photoreceptor cells upon detection of light (Pinto *et al.*, 2007). Homozygous KO mice displayed a 67% decrease in rod-derived (scotopic) ERG response ("a" wave) at the earliest recorded time point, P16, when mice are just opening their eyes (Figure 2A). Rod photoreceptors lacking ARL2BP exhibited a comparable sensitivity to WT at P16 ($I_{1/2}$ = 0.2075 ± 0.02 cd · s m^{-2} (+/+) and 0.241 ± 0.06 cd · s m^{-2} (–/–), with reduced "a"-wave maximum amplitudes of 528.4 μV ± 12.93 μV (+/+) and 179.8 μV ± 10.48 μV (–/–) (Figure 2C). We observed a progressive loss of function with a 90% reduction in rod photoresponse by P210 (Figure 2, A and D). It is important to note that heterozygous mice did not reveal any retinal phenotypes, demonstrating that one WT allele is sufficient for ARL2BP function within the retina.

Similar to rods, cone photoresponses were reduced at P16 and progressively declined as the animals aged (Figure 2B). The ERG reduction seen in 1–base pair deletion animals was analogous to the ERG produced by those with an 8–base pair deletion. The animals with a 6–base pair deletion that led to an in-frame removal of two amino acids (Δ16–17) displayed normal retinal function (Supplemental Figure 2) and served as a control to demonstrate the specificity of the single guide RNA (sgRNA) used to generate the KO mice. Altogether, these results demonstrate the need for ARL2BP in photoreceptor function.

ARL2BP is necessary for photoreceptor cell survival

The early loss in photoreceptor function suggested a possible defect in the development of photoreceptor cells. Therefore, we examined the retinal morphology at P16 by staining retinal cross-sections with the nuclear marker propidium iodide. Interestingly, at P16, when ERG responses are reduced, retinal lamination appears normal in the absence of ARL2BP. Additionally, we observed occasional brightly stained nuclei in the KO sections at P16, indicative of photoreceptor cell death (Figure 3A). The development of inner neurons was normal, as there was no alteration in bipolar or horizontal cell numbers (Supplemental Figure 3).

However, at P210, the majority of photoreceptor nuclei were lost, signifying degeneration of photoreceptor cells in the absence of ARL2BP (Figure 3, B and C, and Supplemental Figure 4). This loss in photoreceptors supported the ERG response at this age (90% reduction), and on the basis of these findings, we conclude that ARL2BP is required for photoreceptor survival.

Loss of ARL2BP induces altered photoreceptor morphology

We considered that the reduced photoreceptor function at P16 could be attributed to a disruption in the phototransduction cascade, either caused by a decrease in protein expression or a change in protein localization. Therefore, we first assessed the expression levels of known phototransduction and OS structural proteins. Immunoblot analysis of P16 retinal lysates revealed a trend for reduction of OS protein levels in ARL2BP KO photoreceptors, including phosphodiesterase-6β (PDE6β), rhodopsin (RHO), transducin (GαT1), and peripherin-2/rds (PRPH-2) (Supplemental Figure 5). In contrast, expression levels of multiple IS proteins remained comparable between WT and KO (Supplemental Figure 5).

Next, we examined the localization of proteins needed for efficient phototransduction and/or OS morphogenesis. We analyzed retinal cross-sections at P16 of WT and KO animals (before photoreceptor degeneration) and found that the localization of multiple OS and IS proteins was maintained in KO photoreceptors, including PDE6β, RHO, cyclic nucleotide-gated channel α1 (CNGA-1), PRPH-2, and GαT1 (Supplemental Figure 6).

There was a uniform reduction in phototransduction proteins and OS structural proteins at P16, which we hypothesize is due to a combination of factors, including shortened OS, photoreceptor cell death, and a consequent degradation of OS proteins. Moreover, because no one OS protein was exclusively reduced, this indicates that phototransduction can still occur, albeit at a reduced strength. This result is supported by the fact that WT and KO mice did not display a major difference in ERG sensitivity or in OS protein localization (Figure 2C and Supplemental Figure 6). Therefore, we hypothesized that ERG reduction was caused by an OS structural defect. This hypothesis was reinforced through light microscopy using toluidine blue–stained retinal sections at P16, which displayed distorted and ragged OSs in the absence of ARL2BP (Figure 4A). For examination of the OS structure in further detail, transmission electron microscopy (TEM) was performed on WT and KO eyecups at P17. In contrast to the well-organized and precisely stacked OS disks seen in

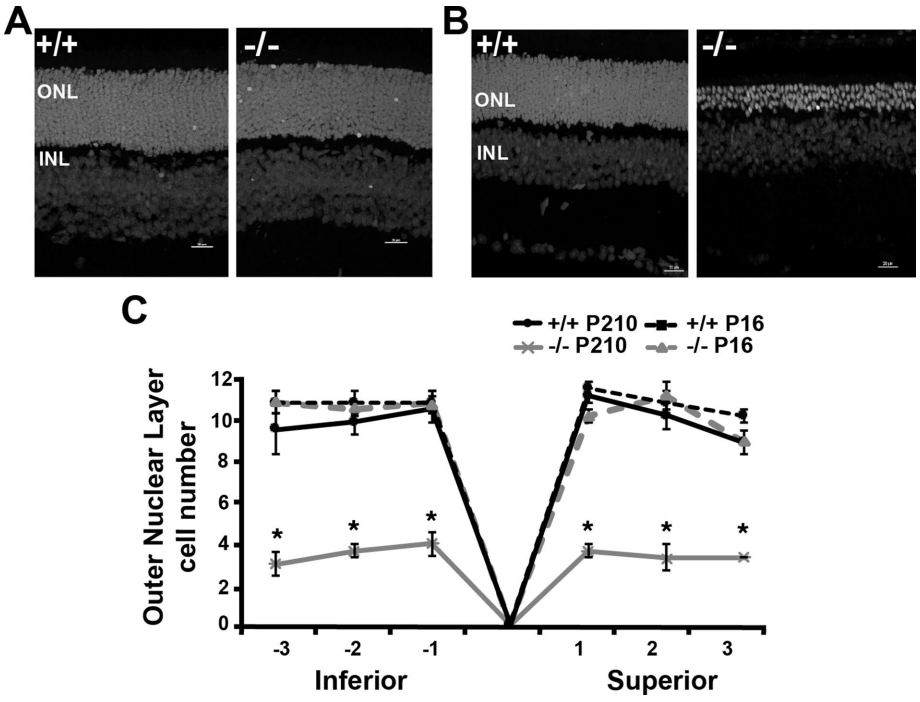

FIGURE 3: Degeneration of photoreceptor cells with loss of ARL2BP. (A, B) Retinal cross-sections of WT (+/+) and KO (–/–) littermates stained with propidium iodide to demonstrate the loss of photoreceptor nuclei in the outer nuclear layer (ONL) at different ages (A, P16) and (B, P210). (C) Quantification of the ONL length (corresponding to the number of nuclei) between +/+ and –/– littermates at different locations within the retina from the inferior (–3) to superior (3) portion at P16 and P210. Scale bar = 20 μm. Data are represented as mean ± SEM ($n = 3$, unpaired two-tailed t test; *, $p < 0.01$). INL, inner nuclear layer; ONL, outer nuclear layer.

WT photoreceptors, KOs displayed dysmorphic OSs, which included misoriented and irregular disks of variable diameters, fragmented OSs, and membranous whorls (Figure 4, B and C). These data demonstrate that loss of ARL2BP impairs photoreceptor disk morphogenesis and causes severe defects in OS structure.

Shortened photoreceptor axonemes in the absence of ARL2BP

Owing to the gross morphological defects in ARL2BP KO photoreceptors, and the presence of ARL2BP in the cilia, we hypothesized that ARL2BP loss could affect ciliary structure. TEM images from longitudinal sections displayed seemingly normal CC ultrastructure in KO retina; unfortunately, the thin sections used for this approach prevent population measurements of ciliary length. We therefore employed fluorescence microscopy, which has been widely used in the photoreceptor field for ensemble measurements of axoneme and CC lengths (Zhao *et al.*, 2003; Liu *et al.*, 2004; Omori *et al.*, 2010; Dilan *et al.*, 2017). The localization of multiple ciliary markers was investigated and the axonemes and CC were measured, using freshly frozen, unfixed eyecups from P16 WT and KO mice. In the absence of ARL2BP, the CC (transition zone) in photoreceptors forms properly, as demonstrated by acetylated tubulin (AcTu) staining (Figure 5A). This result was supported by CC length measurements from WT and KO TEM samples, which were found to be comparable (1.25 μm ± 0.05, $n = 15$, Figure 4C). However, widely used photoreceptor axonemal markers such as RP1 and MAK, revealed a reduction in staining along the distal axoneme (2–3 μm in KO compared with 4–5 μm in WT; Figure 5, A and B), indicating a defect in the extension of the axoneme. One hundred ciliary measurements from three different mice are displayed in violin plots to show the distribution of lengths for RP1, MAK (axoneme), and AcTu (CC) (Figure 5, C–E, respectively), and are quantified in Figure 5F.

Intriguingly, while investigating the localization of multiple ciliary markers, we noticed that staining of retinitis pigmentosa GTPase regulator (RPGR), a photoreceptor-specific cilia-related protein (Meindl *et al.*, 1996; Kirschner *et al.*, 1999), was severely diminished in KO sections at P16 (Figure 5A). Overall, these results indicate a critical role for ARL2BP in the maintenance of photoreceptor axoneme and RPGR localization.

ARL2BP loss disrupts DMT formation

Defects in axonemal extension in ARL2BP-null animals prompted us to assess cross-sections of photoreceptor cilia structure with TEM. We confirmed the formation of 9 + 0 DMTs in photoreceptor CC of KO animals. However, most strikingly, animals lacking ARL2BP displayed abnormal DMT organization, with multiple MTs possessing open B-tubules (Figure 6A). In contrast, open B-tubules were never observed in WT photoreceptor CC. This phenotype is reminiscent of the ARL13b hennin mutant, the only other animal model reported to display this phenotype (Caspary *et al.*, 2007). Upon examination of distal regions in the axoneme, we observed the expected change from doublet to singlet MTs in WT photoreceptors (Figure 6B). However, in the distal regions of KO photoreceptor axonemes, we found a reduced number of singlet structures. Additionally, we were unable to identify a 9 + 0 arrangement of microtubular structures (Figure 6B). This corroborates our findings from RP1 immunostaining, bearing in mind that RP1 is a photoreceptor-specific MT-associated protein that links the OS disks to the axoneme, predominantly in the distal region where singlets are present (Liu *et al.*, 2004) (Figure 5). In conclusion, ARL2BP KO photoreceptors are defective in inner junction B-tubule closure, consequently signifying a role for ARL2BP in photoreceptor DMT formation and axoneme extension.

DISCUSSION

In this study, we generated a global KO of ARL2BP. This animal model phenocopied defects reported in patients with ARL2BP mutations, including the presentation of situs inversus (Davidson *et al.*, 2013). However, the current study focused on the cilia-specific role for ARL2BP in photoreceptor cells. The absence of ARL2BP led to a progressive loss of function and degeneration of photoreceptors. We observed early morphological defects that included abnormal ciliary MT doublet structure with open B-tubules. We hypothesize that abnormal doublet structure likely leads to impaired extension of the photoreceptor distal axoneme and a consequent compromise of disk morphogenesis and OS structure.

ARL2BP is necessary for photoreceptor function

Lack of ARL2BP leads to a decrease in photoreceptor function, even at an early age (P16). Most interestingly, OS disk morphology is affected, with most disks aligned vertically rather than horizontally. We

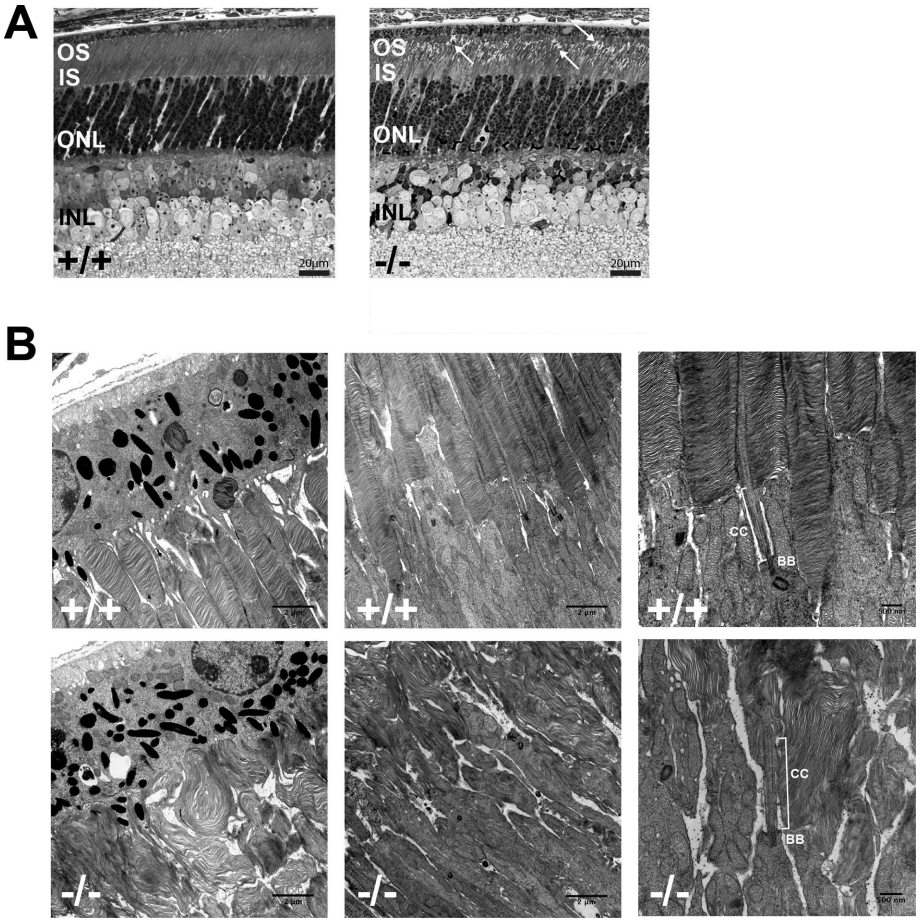

FIGURE 4: Abnormal photoreceptor OS disk morphology in the absence of ARL2BP. (A) Representative toluidine blue–stained retinal cross-sections from WT (+/+) and KO (–/–) littermates at P16. Arrows point to disorganized OSs. Scale bar = 20 μm. (B) Electron micrographs of retinal cross-sections of +/+ and –/– littermates at P16 illustrating the structural abnormalities of the OS in the KO. The left two panels of electron micrographs were taken at lower magnifications (scale bar = 2 μm); the right panel of electron micrographs were taken at a higher magnification (scale bar = 500 nm). BB, basal body; CC, connecting cilium; INL, inner nuclear layer; ONL, outer nuclear layer.

attribute the reduction in photoreceptor function to dysmorphic and shortened OSs. This conclusion is supported by our findings that the sensitivity of photoresponse remains unaltered (Figure 2C) and results that indicate that the phototransduction cascade is intact (Supplemental Figure 5).

Owing to the suggested role for ARL2BP in ciliogenesis and the importance of cilia in protein movement, we originally hypothesized that loss of ARL2BP would affect the trafficking of OS resident proteins. However, OS proteins appear to be properly localized in ARL2BP KO photoreceptors at P16, indicative of normal trafficking (Supplemental Figure 6). We did observe a slight mislocalization of rhodopsin (Supplemental Figure 6C), which we believe is due to the inability of the shortened OS to accommodate the massive rhodopsin protein levels normally present in the OS (Pearring *et al.*, 2013). On the basis of these results, we conclude that OS protein trafficking is not the primary culprit of vision loss in the absence of ARL2BP.

Intriguingly, a few IS resident proteins were found to be mislocalized in ARL2BP KO retina. Specifically, syntaxin 3 (STX3) and receptor expression-enhancing protein 6 were found in the OS of ARL2BP KO retina at P16 (Supplemental Figure 7). This finding for STX3 has been previously shown in BBS mutant models (Datta *et al.*, 2015; Dilan *et al.*, 2017; Hsu *et al.*, 2017), and is thought to indicate a specific role for the BBSome as a gatekeeper in photoreceptor cells. However, ARL2BP does not interact with the BBSome, and absence of ARL2BP does not affect BBSome subunit protein expression (Supplemental Figure 7 and unpublished data). Therefore, we propose that disturbances in the formation or stability of the photoreceptor cilia could also result in IS protein mislocalization.

ARL2BP is indispensable for normal OS morphology

ARL2BP KO photoreceptors displayed highly disorganized OSs, yet BBs and CC of seemingly normal ultrastructure in longitudinal sections. Importantly, however, fluorescence microscopy analysis with axonemal markers revealed that axonemes were shorter with loss of ARL2BP at P16. A decrease in RP1 and MAK staining (axonemal markers) was also seen at P10 (Supplemental Figure 8). These results demonstrate a defect in photoreceptor axoneme extension during development of the OS. Additionally, it has been shown that horizontal disk stacking is disrupted in RP1 KO mouse models (Liu *et al.*, 2003). Thus, it is possible that the vertical disk alignment seen in ARL2BP KO mice may be a direct consequence of the change in RP1, and perhaps other axonemal proteins, primarily caused by unstable or shortened axonemes.

On the basis of our results from ARL2BP KO animals, we envision three possible models for the role of ARL2BP in photoreceptors that we discuss in the following sections.

ARL2BP loss results in ciliary protein mislocalization

RPGR is a ciliary transition-zone protein that has a retina-specific isoform, mutations in which cause X-linked RP (Kirschner *et al.*, 1999). Intriguingly, RPGR localization was severely affected with loss of ARL2BP. RPGR KO mouse models, however, cause a much milder phenotype than what is seen with loss of ARL2BP. It has also been shown that loss of RPGR in combination with the ablation of other ciliary proteins, such as CEP290 and RPGRIP, causes a much more severe defect than with loss of RPGR alone (Hong *et al.*, 2001; Zhao *et al.*, 2003; Anand and Khanna, 2012; Rao *et al.*, 2016). Yet we found both CEP290 and RPGRIP staining unaffected with loss of ARL2BP (Supplemental Figure 9). Therefore, we hypothesize that RPGR mislocalization is a secondary effect of ARL2BP loss, due to structural disruptions of the axoneme, and does not contribute significantly to the phenotype of the ARL2BP KO animals.

Alternatively, we cannot discount the possibility that RPGR and ARL2BP directly interact. However, our attempts to verify an interaction by immunoprecipitation with retinal lysates have failed, making this possibility unlikely.

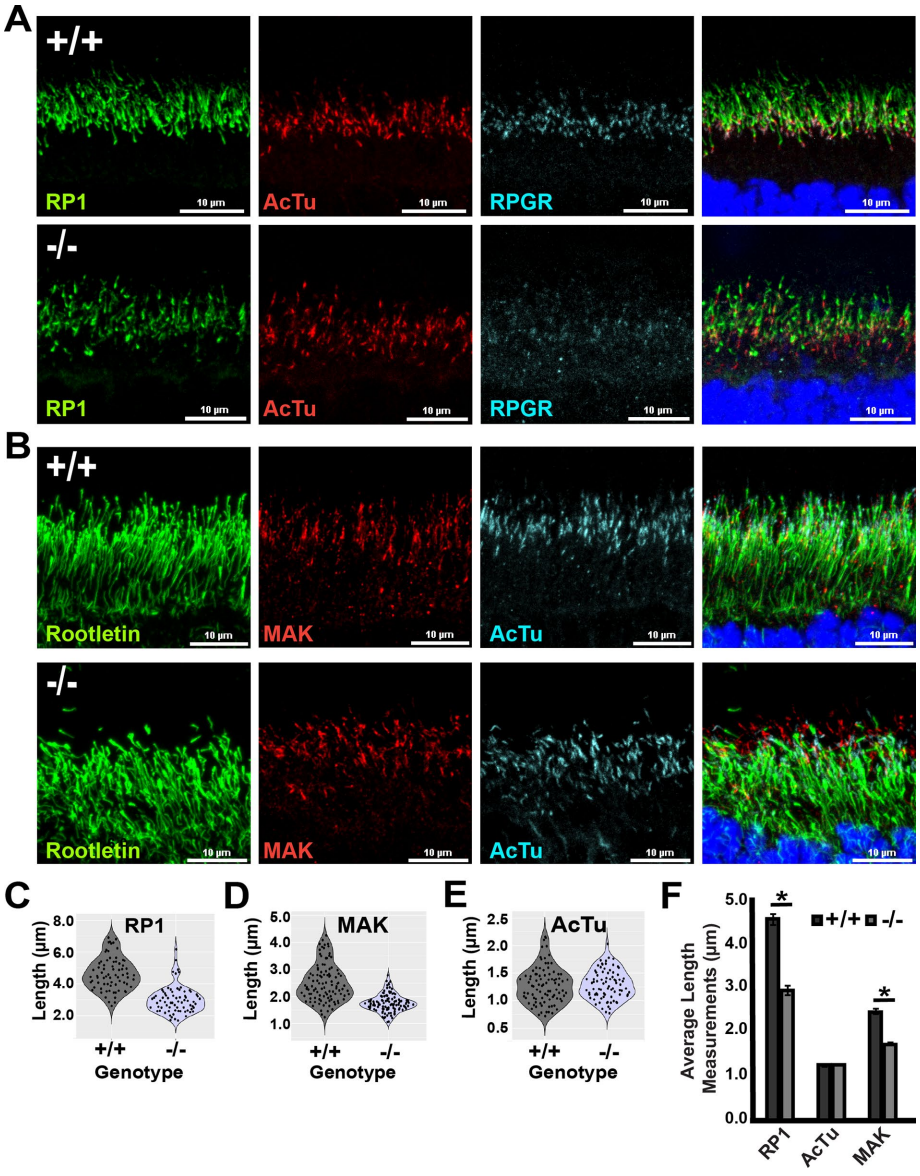

FIGURE 5: ARL2BP is needed for maintenance of photoreceptor axoneme. (A, B) Retinal cross-sections from WT (+/+) and KO (–/–) littermates at P16 showing localization for (A) RP1 (green), acetylated α-tubulin (AcTu, red), and RPGR (cyan) (scale bar = 10 µm) and (B) rootletin (green), MAK (red), and AcTu (cyan) (scale bar = 10 µm). (C–E) Frequency distribution illustrating the percentage of total measured axonemes: (C) length from tip of AcTu to tip of RP1, (D) length from tip of AcTu to tip of MAK, and (E) length from base to tip of AcTu. (F) Quantitation of total measured axonemes and connecting cilia from P16 +/+ and –/–. Data are represented as mean ± SEM ($n = 300$, unpaired two-tailed t test; *, $p < 0.05$).

ARL2BP interaction with ARL2 GTPase affects microtubular axoneme assembly

ARL2BP, or BART, was originally named for its proposed interaction with the small GTPase ARL2 (ADP-ribosylation factor-like 2) (Sharer and Kahn, 1999). Significantly, x-ray crystallography revealed a unique binding conformation between ARL2BP and ARL2-GTP (Zhang *et al.*, 2009). However, our attempts to confirm this interaction in photoreceptors have so far been unproductive (Supplemental Figure 10). Nonetheless, ARL2's known interaction with tubulin and tubulin chaperones (Bhamidipati *et al.*, 2000; Tian *et al.*, 2010; Nithianantham *et al.*, 2015; Francis *et al.*, 2017) prompts a compelling direction of study for the role of ARL2BP in the development and stability of photoreceptor MTs. Therefore, more sensitive assays will be employed to examine their interaction and its importance in photoreceptors.

Impaired DMT assembly with loss of ARL2BP causes instability of axoneme

Our most remarkable discovery concerns the photoreceptor DMT structure of the CC and axoneme, which was abnormal in the absence of ARL2BP. ARL2BP KO photoreceptor CC appears to have lost the inner junction closure, leaving an opening in the B-tubule (Figure 7B). This result is similar to the ARL13b hennin KO, which showed open B-tubules in the primary cilia of embryonic nodes (Caspary *et al.*, 2007). Recent studies on the loss of ARL13b in retina have shown severe photoreceptor dysfunction with no photoresponse, accompanied by complete loss of OS (Hanke-Gogokhia *et al.*, 2017; unpublished data). Given that these models display a more severe phenotype than observed in our studies on ARL2BP, and that ARL13b protein expression and localization was comparable between ARL2BP WT and KO retina (Supplemental Figures 5 and 11), ARL2BP must be uniquely required for DMT formation in ciliary axonemes. It is possible that ARL2BP serves as a component of the inner junction protein complex (which is a nontubulin protofilament; Nicastro *et al.*, 2011; Pigino *et al.*, 2012) or that ARL2BP plays a role in stabilizing DMT structure as an MT-associated protein. It is also possible that ARL2BP is involved in targeting MT-interacting proteins (MIPs) to the DMTs, such as MIP3, a protein known to support the B-tubule structure (Nicastro *et al.*, 2011; Ichikawa *et al.*, 2017).

Furthermore, the loss of singlet MTs in the distal portions of KO photoreceptor axonemes indicates that improper DMT formation results in unstable ciliary extension (Figure 7). Correspondingly, it has been shown that transport along the DMT is A and B specific, wherein dynein motor proteins travel along the A-tubule and kinesin travels along the B-tubule (Stepanek and Pigino, 2016). Any disruption in the anterograde transport (B-tubule specific) of axoneme-building proteins consequently results in the inability of the axoneme to elongate (Prevo *et al.*, 2017). Therefore, we hypothesize that the impairment in ciliary extension seen with loss of ARL2BP disrupts the ability of photoreceptors to form properly stacked OS disks (scheme illustrated in Figure 7, A and B).

Our studies show the need for ARL2BP in DMT formation and core axoneme structure and elongation. The study of ARL2BP also highlights the importance of axoneme structure and stability in OS disk formation. How changes in the DMT and axoneme structure lead to altered photoreceptor OS organization and function will

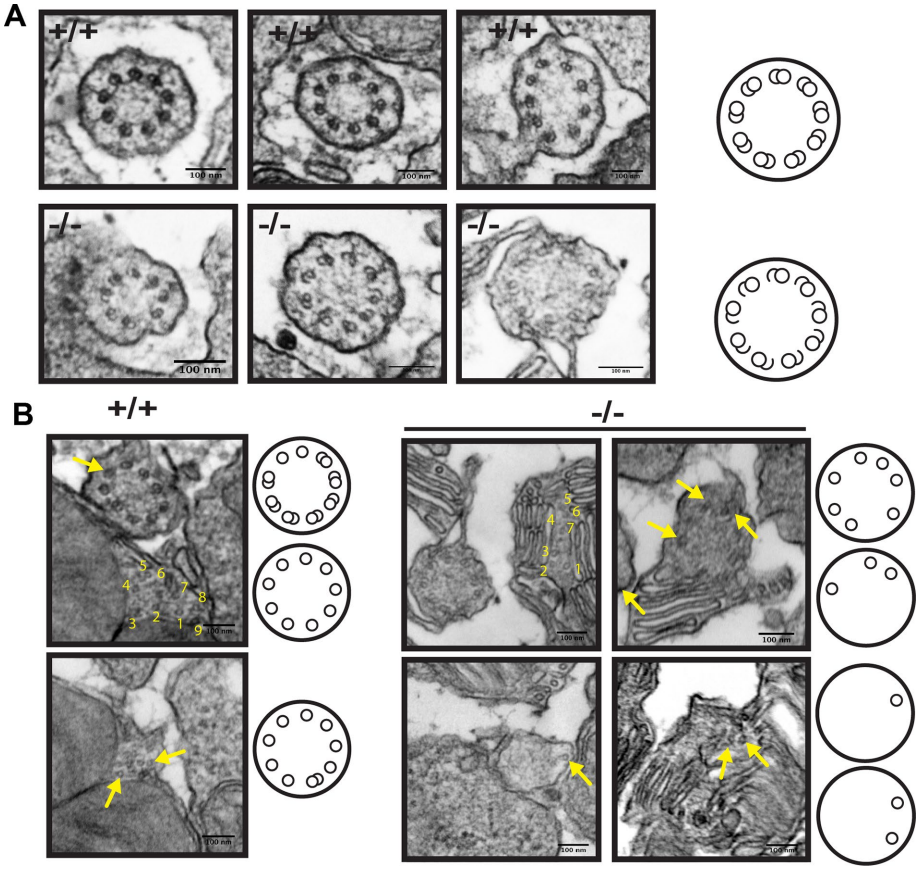

FIGURE 6: ARL2BP is required for normal doublet and singlet MT formation in photoreceptors. (A, B) Cross-sectional transmission electron micrographs from WT (+/+) and KO (–/–) retina at P16 illustrating the (A) structural defects in DMTs of the –/– photoreceptor CC, displaying open B-tubules (scale bar = 100 nm), and (B) singlet and DMTs present in more distal regions of the axoneme. The +/+ sections (left) illustrate 9 singlet MTs in both sections shown, whereas –/– sections never displayed 9 singlets. Numbers and arrows refer to singlets (scale bar = 100 nm).

provide exciting insight into photoreceptor biology as well as ciliopathy-related fields.

MATERIALS AND METHODS

Generation of mouse model and genotyping

The generation and cloning of the targeted sgRNA was performed as described in Yang *et al.* (2013). Briefly, 20-nt sgRNA oligonucleotides (Supplemental Table 2) specific for a region in exon 2 of ARL2BP immediately upstream of the 5′–NGG protospacer adjacent motif (PAM) sequence were annealed and ligated into pX330 vector (pSpCas9). Upon DNA purification, the T7 promoter was added to the sgRNA template by PCR amplification (primer is shown in Supplemental Table 2). Following gel extraction, the T7-sgRNA template was used for in vitro transcription using a kit from Clontech. The sgRNA was then purified using an RNA purification kit from Ambion. The specificity and efficacy of the sgRNA/Cas9 cutting was confirmed by in vitro assays. Both the sgRNA and Cas9 mRNA (Invitrogen) were injected into the pronuclei of FVB blastocysts (17 and 34 ng/μl, respectively). The correctly targeted founders were identified by sequencing of the genomic DNA fragment surrounding the ARL2BP exon 2 region (Supplemental Table 2). The mice were then backcrossed into C57black 6/J to remove the *rd1* allele naturally present in FVB mice. However, multiple backcrosses into the C57black 6/J strain led to concomitant reduction in the number of KO animals obtained. Therefore, mice were crossed into 129/SV-E mice (Strain #476 from Charles River Laboratories), which somewhat restored the expected Mendelian ratios of KO animals obtained from heterozygous crosses. Owing to the extensive backcrossing (eight total rounds), we could rule out "off-target" effects sometimes associated with Crispr-Cas9 gene editing. Genotyping was performed using primers listed in Supplemental Table 2 on ear-punch samples, and the PCR fragments were analyzed by capillary electrophoresis or by 7% polyacrylamide/urea gels followed by detection with the Li-Cor Odyssey system. The Institutional Animal Care and Use Committee of the West Virginia University approved all experimental procedures involving animals conducted in this study.

Generation of antibody against full-length ARL2BP

ARL2BP antibody was generated as previously described (Wright *et al.*, 2016). Briefly, ARL2BP with a C-terminal his-tag was expressed in Origami *Escherichia coli* strain (Novagen). Origami cells were grown to an $OD_{600} \approx 0.7$, and protein production was induced with 0.5 mM isopropyl β-D-1-thiogalactopyranoside for 18 h at 16°C. The protein was purified from the soluble fraction using a nickel his-affinity column, and the eluate was supplied to Pacific Immunology for generation of the antibody in rabbits. Antibody serum was then purified against a column cross-linked with GST-ARL2BP fusion protein and tested via immunoblotting in both HEK 293 cells expressing ARL2BP and retinal extracts.

Immunoblotting

Mice were killed by CO_2 inhalation followed by cervical dislocation, and eyes were enucleated. Following dissection, flash-frozen retinas were sonicated in phosphate-buffered saline (PBS; 137 mM NaCl, 2.7 mM KCl, 4.3 mM $Na_2HPO_4{\cdot}7H_2O$, 1.4 mM KH_2PO_4, with protease inhibitor cocktail [Roche]), and protein concentrations were measured using a NanoDrop spectrophotometer (Thermo Fisher Scientific). Equal amounts of samples (100 μg total protein per well) were separated on a polyacrylamide SDS–PAGE and transferred onto polyvinylidene difluoride membranes (Immunobilon-FL; Millipore, Billerica, MA). Membranes were blocked with Western blot blocking buffer (Rockland) for 30 min at room temperature and incubated with primary antibodies overnight at 4°C (antibody dilutions shown in Supplemental Table 1). Blots were washed in PBST (PBS with 0.1% Tween-20) three times for 5 min (3 × 5 min) at room temperature and incubated in secondary antibody, goat anti-rabbit Alexa Fluor 680, goat anti-rat Alexa Fluor 680, or goat anti-mouse Alexa Fluor 800 (Invitrogen) for 30 min at room temperature. After 3 × 5 min of washes with PBST, membranes were scanned using the Odyssey Infrared Imaging System (Li-Cor Biosciences, Lincoln, NE).

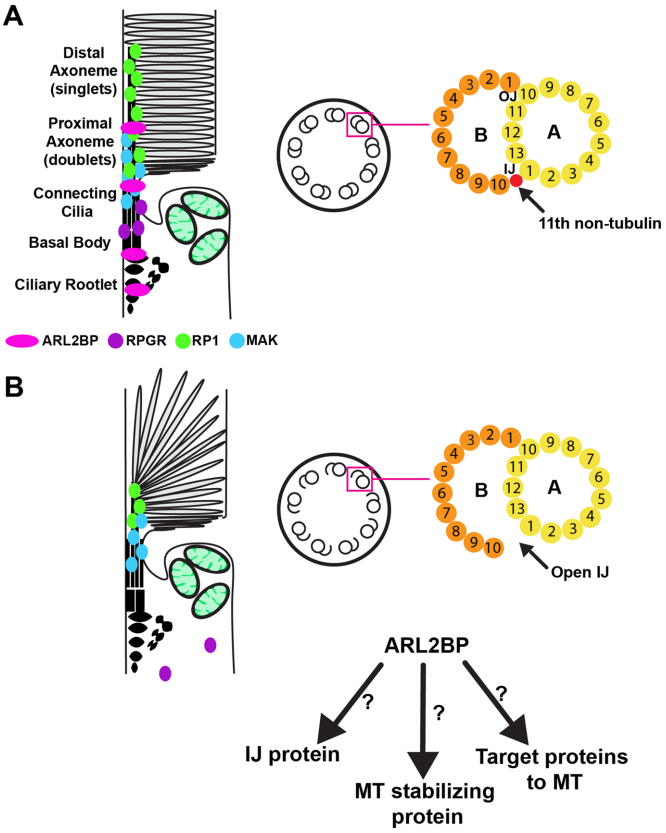

FIGURE 7: Role for ARL2BP in photoreceptors. (A, B) Scheme illustrating the role of ARL2BP in photoreceptor microtubular axoneme extension, OS disk alignment, and ciliary protein localization. (A) With ARL2BP, photoreceptor OS develops normally, with correct DMT formation, axoneme extension, and disk alignment. (B) Without ARL2BP, axonemes are shorter, OS disks are not properly stacked, and DMT formation is disrupted—indicating a role for ARL2BP in DMT formation and/or stability. IJ, inner junction; MT, microtubule; OJ, outer junction.

Immunofluorescence

Enucleated eyes were immersed in 4% paraformaldehyde (PFA) fixative for 15 min before removal of the cornea and lens. Eyecups were fixed for a total of 2 h and washed in 1X PBS for 20 min, followed by incubation in 20% sucrose/PBS overnight at 4°C. Afterward, eyes were incubated in a 1:1 mixture of 20% sucrose in PBS and OCT (Cryo Optimal Cutting Temperature Compound; Sakura) for 1 h and flash-frozen in OCT.

To stain specifically for cilia in photoreceptor cells, eyes were fixed for 30 s in 4% PFA after removal of anterior segments and washed in 1X PBS for 1 min. They were then immediately flash-frozen in OCT.

Cryosectioning was performed with a Leica CM1850 Cryostat, and serial retinal sections of 16 or 12 µm (for cilia) thickness were mounted on Superfrost Plus slides (Fisher Scientific). Retinal sections mounted on slides were washed with 1X PBS and incubated for 1 h in blocking buffer (PBS with 5% goat sera, 0.5% Triton X-100, 0.05% sodium azide). Retinal sections were then incubated with primary antibody overnight at 4°C (dilutions defined in Supplemental Table 1), followed by two 15 min washes with PBSTx (1X PBS with 0.1% Triton X-100), and one with PBS 1x before incubation with secondary antibody at 1:1000 dilution for 1 h. After three 15 min washes with PBSTx, the sections were mounted with ProLong Gold antifade reagent (Life Technologies) and viewed on a Nikon Eclipse T*i* C2 confocal microscope using excitation wavelengths of 405, 488, 543, and 647 nm.

For propidium iodide staining, retinal sections were incubated with propidium iodide for 1 h at room temperature following blocking. They were then washed three times for 15 min with PBSTx.

TEM

Before enucleation, transcardial perfusions were performed on the mice for 10 min using 15 ml of 2% PFA, 2% glutaraldehyde, and 0.05% $CaCl_2$ in 50 mM MOPS buffer. Once the perfusion was completed, the cornea and lens were removed from enucleated eyes and kept in fixative for 1 h. Dissection, embedding, and TEM was completed according to previously published methods (Ku *et al.*, 2015).

ERG

Mice were dark-adapted overnight before testing. Mice were anesthetized (2.0% isoflourane with 2.5 l/min [lpm] oxygen flow rate) for 10 min. Test subject eyes were topically dilated with a 1:1 mixture of tropicamide:phenylephrine hydrochloride. Mice were placed on a heated platform with a continuous flow of isoflourane anesthesia through a nose cone (1.5% isoflourane with 2.5 lpm oxygen flow rate). A reference electrode was placed subcutaneously in the scalp, and ERG responses were recorded from both eyes with silver wire electrodes placed above each cornea, with contact being made with a drop of hypromellose solution (2% hypromellose in PBS) (Gonioscopic Prism Solution; Wilson Ophthalmic, Mustang, OK). Rod-dominated responses (scotopic) were elicited in the dark with flashes of LED white light at increasing flash intensities. Light-adapted cone responses (photopic) were elicited with white light flashes in the presence of a 30 cd/m^2 rod-saturating white background light. ERGs were performed on the UTAS Visual Diagnostic System with BigShot Ganzfeld with UBA-4200 amplifier and interface, and EMWIN version 9.0.0 software (LKC Technologies, Gaithersburg, MD).

Subretinal injections

Plasmid DNA was injected and electroporated into the subretinal space of P0 mice according to a previously published protocol (Venkatesh *et al.*, 2013). DNA solutions were prepared at 5 µg/µl. Each animal received 0.5 µl of DNA in the right eye, and no injection in the untreated contralateral eye.

Statistical analysis

All data are presented as mean ± standard error margin. ERG data and immunoblots (Supplemental Material) were analyzed by unpaired, two-tailed *t* test ($n = 3$ or 4). For ciliary measurements, 80–100 cilia were measured for each animal ($n = 3$), and data were visualized with the ggplot2 package in R version 3.3.2. Image and densitometry analyses were performed using ImageJ version 1.50i.

ACKNOWLEDGMENTS

We thank the Transgenic Core at West Virginia University for help with the generation of the ARL2BP knockout model, Peter Stoilov, Zachary Wright (West Virginia University), and Tamara Caspary (Emory University) for help with data collection and analysis, Jessica Cunningham (West Virginia University) for help with transcardial perfusions, and Paolo Fagone (West Virginia University Protein Core) for help with the purification of ARL2BP protein. This work was supported by National Institutes of Health grants R01 EY028035 (to V.R.), R01 EY025536 (to V.R. and Peter Stoilov), R21 EY027707 (to V.R.), EY025291(to A.F.X.G.), and the West Virginia Lions and Lions Club International Foundation.

REFERENCES

Anand M, Khanna H (2012). Ciliary transition zone (TZ) proteins RPGR and CEP290: role in photoreceptor cilia and degenerative diseases. Expert Opin Ther Targets 16, 541–551.

Bhamidipati A, Lewis SA, Cowan NJ (2000). ADP ribosylation factor-like protein 2 (Arl2) regulates the interaction of tubulin-folding cofactor D with native tubulin. J Cell Biol 149, 1087–1096.

Boldt K, Mans DA, Won J, van Reeuwijk J, Vogt A, Kinkl N, Letteboer SJ, Hicks WL, Hurd RE, Naggert JK, *et al*. (2011). Disruption of intraflagellar protein transport in photoreceptor cilia causes Leber congenital amaurosis in humans and mice. J Clin Invest 121, 2169–2180.

Brown P, Gibbons I, Wald G (1963). The visual cells and visual pigment of the mudpuppy, *Necturus*. J Cell Biol 19, 79–106.

Bujakowska KM, Liu Q, Pierce EA (2017). Photoreceptor cilia and retinal ciliopathies. Cold Spring Harb Perspect Biol 9, a028274.

Caspary T, Larkins CE, Anderson KV (2007). The graded response to Sonic Hedgehog depends on cilia architecture. Dev Cell 12, 767–778.

Datta P, Allamargot C, Hudson JS, Andersen EK, Bhattarai S, Drack AV, Sheffield VC, Seo S (2015). Accumulation of non-outer segment proteins in the outer segment underlies photoreceptor degeneration in Bardet–Biedl syndrome. Proc Natl Acad Sci USA 112, E4400–E4409.

Davidson AE, Schwarz N, Zelinger L, Stern-Schneider G, Shoemark A, Spitzbarth B, Gross M, Laxer U, Sosna J, Sergouniotis PI, *et al*. (2013). Mutations in ARL2BP, encoding ADP-ribosylation-factor-like 2 binding protein, cause autosomal-recessive retinitis pigmentosa. Am J Hum Genet 93, 321–329.

Dilan TL, Singh RK, Saravanan T, Moye A, Goldberg AFX, Stoilov P, Ramamurthy V (2017). Bardet-Biedl Syndrome-8 (BBS8) protein is crucial for the development of outer segments in photoreceptor neurons. Hum Mol Genet 27, 283–294.

Francis JW, Goswami D, Novick SJ, Pascal BD, Weikum ER, Ortlund EA, Griffin PR, Kahn RA (2017). Nucleotide binding to ARL2 in the TBCD·ARL2·β-tubulin complex drives conformational changes in β-tubulin. J Mol Biol 429, 3696–3716.

Goldberg AFX, Moritz OL, Williams DS (2016). Molecular basis for photoreceptor outer segment architecture. Prog Retin Eye Res 55, 52–81.

Hanke-Gogokhia C, Wu Z, Sharif A, Yazigi H, Frederick JM, Baehr W (2017). The guanine nucleotide exchange factor, Arf-like protein 13b, is essential for assembly of the mouse photoreceptor transition zone and outer segment. J Biol Chem 292, 21442–21456.

Hong DH, Yue G, Adamian M, Li T (2001). Retinitis pigmentosa GTPase regulator (RPGRr)-interacting protein is stably associated with the photoreceptor ciliary axoneme and anchors RPGR to the connecting cilium. J Biol Chem 276, 12091–12099.

Hsu Y, Garrison JE, Kim G, Schmitz AR, Searby CC, Zhang Q, Datta P, Nishimura DY, Seo S, Sheffield VC (2017). BBSome function is required for both the morphogenesis and maintenance of the photoreceptor outer segment. PLoS Genet 13, e1007057.

Ichikawa M, Liu D, Kastritis PL, Basu K, Hsu TC, Yang S, Bui KH (2017). Subnanometre-resolution structure of the doublet microtubule reveals new classes of microtubule-associated proteins. Nat Commun 8, 15035.

Insinna C, Pathak N, Perkins B, Drummond I, Besharse JC (2008). The homodimeric kinesin, Kif17, is essential for vertebrate photoreceptor sensory outer segment development. Dev Biol 316, 160–170.

Kirschner R, Rosenberg T, Schultz-Heienbrok R, Lenzner S, Feil S, Roepman R, Cremers FP, Ropers HH, Berger W (1999). RPGR transcription studies in mouse and human tissues reveal a retina-specific isoform that is disrupted in a patient with X-linked retinitis pigmentosa. Hum Mol Genet 8, 1571–1578.

Knabe W, Kuhn H (1997). Ciliogenesis in photoreceptor cells of the tree shrew retina. Anat Embryol (Berl) 196, 123–131.

Ku CA, Chiodo VA, Boye SL, Hayes A, Goldberg AF, Hauswirth WW, Ramamurthy V (2015). Viral-mediated vision rescue of a novel AIPL1 cone-rod dystrophy model. Hum Mol Genet 24, 670–684.

Linck R, Fu X, Lin J, Ouch C, Schefter A, Steffen W, Warren P, Nicastro D (2014). Insights into the structure and function of ciliary and flagellar doublet microtubules: tektins, Ca^{2+}-binding proteins, and stable protofilaments. J Biol Chem 289, 17427–17444.

Linck RW, Stephens RE (2007). Functional protofilament numbering of ciliary, flagellar, and centriolar microtubules. Cell Motil Cytoskeleton 64, 489–495.

Liu Q, Lyubarsky A, Skalet JH, Pugh EN, Pierce EA (2003). RP1 is required for the correct stacking of outer segment discs. Invest Ophthalmol Vis Sci 44, 4171–4183.

Liu Q, Zuo J, Pierce EA (2004). The retinitis pigmentosa 1 protein is a photoreceptor microtubule-associated protein. J Neurosci 24, 6427–6436.

May-Simera H, Nagel-Wolfrum K, Wolfrum U (2017). Cilia—the sensory antennae in the eye. Prog Retin Eye Res 60, 144–180.

Meindl A, Dry K, Herrmann K, Manson E, Ciccodicola A, Edgar A, Carvalho MRS, Achatz H, Hellebrand H, Lennon A, *et al*. (1996). A gene (RPGR) with homology to the RCC1 guanine nucleotide exchange factor is mutated in X-linked retinitis pigmentosa (RP3). Nat Genet 13, 35.

Molday RS, Moritz OL (2015). Photoreceptors at a glance. J Cell Sci 128, 4039–4045.

Nicastro D, Fu X, Heuser T, Tso A, Porter ME, Linck RW (2011). Cryo-electron tomography reveals conserved features of doublet microtubules in flagella. Proc Natl Acad Sci USA 108, E845–E853.

Nithianantham S, Le S, Seto E, Jia W, Leary J, Corbett KD, Moore JK, Al-Bassam J (2015). Tubulin cofactors and Arl2 are cage-like chaperones that regulate the soluble alphabeta-tubulin pool for microtubule dynamics. Elife 4, 1–33.

Omori Y, Chaya T, Katoh K, Kajimura N, Sato S, Muraoka K, Ueno S, Koyasu T, Kondo M, Furukawa T (2010). Negative regulation of ciliary length by ciliary male germ cell-associated kinase (Mak) is required for retinal photoreceptor survival. Proc Natl Acad Sci USA 107, 22671–22676.

Pearring JN, Salinas RY, Baker SA, Arshavsky VY (2013). Protein sorting, targeting and trafficking in photoreceptor cells. Prog Retin Eye Res 36, 24–51.

Pierce EA, Quinn T, Meehan T, McGee TL, Berson EL, Dryja TP (1999). Mutations in a gene encoding a new oxygen-regulated photoreceptor protein cause dominant retinitis pigmentosa. Nat Genet 22, 248–254.

Pigino G, Maheshwari A, Bui KH, Shingyoji C, Kamimura S, Ishikawa T (2012). Comparative structural analysis of eukaryotic flagella and cilia from *Chlamydomonas*, *Tetrahymena*, and sea urchins. J Struct Biol 178, 199–206.

Pinto LH, Invergo B, Shimomura K, Takahashi JS, Troy JB (2007). Interpretation of the mouse electroretinogram. Doc Ophthalmol 115, 127–136.

Prevo B, Scholey JM, Peterman EJG (2017). Intraflagellar transport: mechanisms of motor action, cooperation, and cargo delivery. FEBS J 284, 2905–2931.

Ramamurthy V, Cayouette M (2009). Development and disease of the photoreceptor cilium. Clin Genet 76, 137–145.

Rao KN, Zhang W, Li L, Ronquillo C, Baehr W, Khanna H (2016). Ciliopathy-associated protein CEP290 modifies the severity of retinal degeneration due to loss of RPGR. Hum Mol Genet 25, 2005–2012.

Sharer JD, Kahn RA (1999). The ARF-like 2 (ARL2)-binding protein, BART. Purification, cloning, and initial characterization. J Biol Chem 274, 27553–27561.

Steinberg R, Wood I (1975). Clefts and microtubules of photoreceptor outer segments in the retina of the domestic cat. J Ultrastructural Res 51, 397–403.

Stepanek L, Pigino G (2016). Microtubule doublets are double-track railways for intraflagellar transport trains. Science 352, 721.

Tian G, Thomas S, Cowan NJ (2010). Effect of TBCD and its regulatory interactor Arl2 on tubulin and microtubule integrity. Cytoskeleton (Hoboken) 67, 706–714.

Venkatesh A, Ma S, Langellotto F, Gao G, Punzo C (2013). Retinal gene delivery by rAAV and DNA electroporation. Curr Protoc Microbiol Chapter 14, Unit-14D.4.

Wensel TG, Zhang Z, Anastassov IA, Gilliam JC, He F, Schmid MF, Robichaux MA (2016). Structural and molecular bases of rod photoreceptor morphogenesis and disease. Prog Retin Eye Res 55, 32–51.

Wright ZC, Singh RK, Alpino R, Goldberg AFX, Sokolov M, Ramamurthy V (2016). ARL3 regulates trafficking of prenylated phototransduction proteins to the rod outer segment. Hum Mol Genet 25, 2031–2044.

Yang H, Wang H, Shivalila CS, Cheng AW, Shi L, Jaenisch R (2013). One-step generation of mice carrying reporter and conditional alleles by CRISPR/Cas-mediated genome engineering. Cell 154, 1370–1379.

Young RW (1967). The renewal of photoreceptor cells outer segments. J Cell Biol 33, 61–72.

Zhang T, Li S, Zhang Y, Zhong C, Lai Z, Ding J (2009). Crystal structure of the ARL2-GTP-BART complex reveals a novel recognition and binding mode of small GTPase with effector. Structure 17, 602–610.

Zhao Y, Hong D-H, Pawlyk B, Yue G, Adamian M, Grynberg M, Godzik A, Li T (2003). The retinitis pigmentosa GTPase regulator (RPGR)- interacting protein: subserving RPGR function and participating in disk morphogenesis. Proc Natl Acad Sci USA 100, 3965–3970.

Zhou C, Cunningham L, Marcus AI, Li Y, Kahn RA (2006). Arl2 and Arl3 regulate different microtubule-dependent processes. Mol Biol Cell 17, 2476–2487.